Cardiac re-entry dynamics and self-termination in DT-MRI based model of Human Foetal Heart

frontiers

Cardiac re-entry dynamics and self-termination in DT-MRI based model of Human Foetal Heart

Irina V. Biktasheva [1,2,*], **Richard A. Anderson** [3], **Arun V. Holden** [4], **Eleftheria Pervolaraki** [4] **and Fen Cai Wen** [1]

[1] *Department of Computer Science, University of Liverpool, Liverpool, UK*
[2] *CEMPS, University of Exeter, Exeter, UK*
[3] *MRC Centre for Reproductive Health, University of Edinburgh, Edinburgh, UK*
[4] *School of Biomedical Sciences, University of Leeds, Leeds, UK*

Correspondence*:
Dr Irina V. Biktasheva
ivb@liverpool.ac.uk

ABSTRACT

The effect of human foetal heart geometry and anisotropy on anatomy induced drift and self-termination of cardiac re-entry is studied here in MRI based 2D slice and 3D whole heart computer simulations. Isotropic and anisotropic models of 20 weeks of gestational age human foetal heart obtained from $100\mu m$ voxel diffusion tensor MRI data sets were used in the computer simulations. The fiber orientation angles of the heart were obtained from the orientation of the DT-MRI primary eigenvectors. In a spatially homogeneous electrophysiological monodomain model with the DT-MRI based heart geometries, cardiac re-entry was initiated at a prescribed location in a 2D slice, and in the 3D whole heart anatomy models. Excitation was described by simplified FitzHugh-Nagumo kinetics. In a slice of the heart, with propagation velocity twice as fast along the fibres than across the fibers, DT-MRI based fiber anisotropy changes the re-entry dynamics from pinned to an anatomical re-entry. In the 3D whole heart models, the fiber anisotropy changes cardiac re-entry dynamics from a persistent re-entry to the re-entry self-termination. The self-termination time depends on the re-entry's initial position. In all the simulations with the DT-MRI based cardiac geometry, the anisotropy of the myocardial tissue shortens the time to re-entry self-termination several folds. The numerical simulations depend on the validity of the DT-MRI data set used. The ventricular wall showed the characteristic transmural rotation of the helix angle of the developed mammalian heart, while the fiber orientation in the atria was irregular.

Keywords: cardiac arrhythmias, anatomically realistic modeling, anisotropy, anatomy induced drift, FitzHugh-Nagumo model

1 INTRODUCTION

Since the over a century ago hypothesis that cardiac re-entry underlies cardiac arrhythmias (Mines, 1913; Garey, 1914) , and the much later confirmation of the hypothesis in cardiac tissue experiment (Allessie et al., 1973; Pertsov et al., 1993), the re-entry (*aka* spiral wave in 2D, cardiac excitation vortex in 3D), its origin and its role in sustained arrhythmias and fibrillation, as well as a possibility of its effective

control and defibrillation, have been an object of extensive theoretical study and modelling (Wiener and Rosenblueth, 1946; Balakhovsky, 1965; Krinsky, 1968; Panfilov et al., 1984; Davydov et al., 1988; Keener, 1988; Ermakova et al., 1989; Biktashev and Holden, 1994; Biktashev, 1998; Fenton and Karma, 1998; Pertsov et al., 2000; Wellner et al., 2002; Biktasheva and Biktashev, 2003; Biktashev et al., 2010, 2011; Biktasheva et al., 2015). From experiment, it is an established point of view that cardiac arrhythmias are due to a complex combination of electrophysiological (Bosch and Nattel, 2002; Workman et al., 2008; Kushiyama et al., 2016), structural (Pellman et al., 2010; Eckstein et al., 2011; Takemoto et al., 2012; Eckstein et al., 2013), and anatomical (MacEdo et al., 2010; Anselmino et al., 2011) factors which sustain cardiac re-entry (Gray et al., 1996; Wu et al., 1998; Nattel, 2002; Yamazaki et al., 2012).

The specific effect of the heart anisotropy and anatomy on cardiac re-entry dynamics is well appreciated (Bishop et al., 2010, 2011; Bishop and Plank, 2012; Fukumoto et al., 2016), and has been studied in simplified mathematical and computer models (Fenton and Karma, 1998; Pertsov et al., 2000; Wellner et al., 2002; Rodriguez et al., 2006; Dierckx et al., 2013). The anisotropic discontinuities in the heart muscle have been commonly seen as a substrate for rise of cardiac re-entry due to the abrupt change in conduction velocity and wavefront curvature(Fenton and Karma, 1998; Spach, 2001; Smaill et al., 2004). On the other hand, extensive mapping of cardiac myocyte orientation in mammalian hearts has shown that the transmural fiber arrangement, including the range of transmural change in fiber angle in ventricular wall, was consistent within a species, and varied between species (Hunter et al., 1997, p. 173). So that the anisotropic discontinuities observed in healthy hearts, and shown to be consistent within a species, might have been suspected to facilitate initiation of arryhthmias.

With the recent advance in DT-MRI technology and in High Performance Computing (HPC), the DT-MRI data sets, including anatomy and myofiber structure, can now be directly incorporated into anatomically realistic computer simulations (Vigmond et al., 2009; Bishop et al., 2010; Antonioletti et al., 2017), so that the anisotropy of the tissue in the *in-silico* model can be switched on and off for the comparison between the isotropic and anisotropic conduction, in order to see the specific anatomy effects, as well as the interplay between the anatomy and anisotropy of an individual heart.

In this paper, we present DT-MRI based anatomically and myofiber structure realistic computer simulation study of cardiac re-entry dynamics in the *in-silico* model of human foetal heart. The raw DT-MRI data (Pervolaraki et al., 2013) was segmented into the tissue/non-tissue pixels based on the MRI luminosity threshold, followed by the calculation of the fiber angles at each voxel from the diffusion-weighted DT-MRI images. The DT-MRI yields 3 eigenvalues, the primary (largest) eigenvalue was used to define local fibre orientations in the simulation study.

The main objectives are to clarify: i) whether the anatomical settings of the foetal heart might support a positive filament tension re-entry, and ii) what would it be the role of the heart anisotropy in that case. Here we demonstrate that anisotropy of the foetal heart rather facilitates self-termination of cardiac re-entry. In a 2D slice of the heart, the fiber anisotropy might change dynamics of the re-entry from pinned to anatomical re-entry. In the full 3D DT-MRI based model, depending on the location of re-entry initiation, the isotropic geometry of the heart might sustain perpetual re-entry even with a positive filament tension kinetics. While the same positive filament tension re-entry initiated at the same location of the foetal heart with the fiber anisotropy self-terminates within a fraction of the rotation period. Time of re-entry self-termination depends on the re-entry initial position. Anisotropy of the real heart speeds up re-entry self-termination. The geometry and anisotropy of the heart together ensure the fastest self-termination of cardiac re-entry.

The novel significance of our findings is that we demonstarte that the heart anisotropy might have rather anti-arrhythmic function as it facilitates fast self-termination of cardiac re-entry. A general role of fiber anisotropy in the genesis and sustenance of arrhythmias could be addressed by numerics even on idealised and simplified geometries with different spatial distributions of anisotropy. The biomedical question addressed in the manuscript is whether self-terminating ventricular arrhythmias can occur in a developing foetal heart, as has inferred from fECG data in (Benson et al., 2015).

2 MATERIALS AND METHODS

2.1 DT-MRI data sets

Tissue acquisition followed medical termination of pregnancy with written and informed consent, and Ethical approval from Lothian Research Ethics Committee (reference 08/S1101/1). Temporary storage of the tissue for imaging was in premises licensed under the UK 2004 Human Tissues Act.

The DT-MRI data set used in this study was of a 143 days gestational age (DGA) human foetal heart described in (Pervolaraki et al., 2013). It was selected as by 143 days the smooth, transmural 120° transmural rotation in helix fiber angle is well established (Pervolaraki et al., 2013; Mekkaoui et al., 2013; Pervolaraki et al., 2017). The heart was immersed in formalin shortly after dissection, and imaged in fomblin after two weeks in formalin.

MRI acquisition was performed in a Bruker Biospin (Ettlingen, Germany) 9.4 Tesla vertical NMR/S System with a $22mm$ imaging coil for Hydrogen (1 H). A three-dimensional diffusion weighted spin echo sequence was carried out at 20°C with $0.1mm^2$ resolution, echo time = $15ms$, repetition time = $500ms$, with 6 averages and a b value of $1000s/mm^2$. In each scan, diffusion weighted images were obtained in 12 directions. The average scan time was 24 hours.

2.2 DT-MRI based anatomy model

Figure 1 shows a cross section of the 143 days of gestational age (DGA) foetal heart, with the already formed intramural myolaminar structure, and yet a bit irregular surface epicardial, endocardial, and septal fibers, see also Figure 4 in (Pervolaraki et al., 2013, p. 5) for the color-encoded fractional anisotropy (FA) and all the three components of the fiber angles in the human foetal heart. While in an adult heart, pinning of cardiac re-entry to endocardium structures such as pectinate muscles junction with crystae terminalis had been previously reported (Wu et al., 1998; Yamazaki et al., 2012; Kharche et al., 2015a). The DT-MRI based foetal heart model offered a unique opportunity to see whether the 20 weeks of gestation age intramural heart structure was capable to support cardiac re-entry, because at that foetal development stage it would not be possible yet for the re-entry to pin to the endocardium fine features, for these anatomical structures were yet to be developed later.

The DT-MRI data sets of the $128 \times 128 \times 128$ voxels size, with voxel resolution of $\sim 100\mu m$, of 143 days of gestational age (DGA) human foetal heart (Pervolaraki et al., 2013), were converted into the BeatBox (Antonioletti et al., 2017) regular Cartesian mesh `.bbg` geometry format, containing the DT-MRI Cartesian coordinates of the heart tissue points together with the corresponding components of the diffusion tensor primary eigenvectors (Antonioletti et al., 2017). The `.bbg` file is an ASCII text file, each line in which describes a point in a regular mesh in the following format:

```
x,y,z,status,fibre_x,fibre_y,fibre_z
```

Figure 1. The 143 DGA human foetal heart (Pervolaraki et al., 2013). BeatBox (Antonioletti et al., 2017) geometry `.bbg` format visualisation with projections of the unit vectors of the local fibre orientation onto the cross-section plane: a smooth intramural fibre distribution has developed, with some surface irregular fibers from earlier developmental stages, as seen in Figure 4 (Pervolaraki et al., 2013, p. 5).

Here `x, y, z` are integer Cartesian coordinates of a DT-MRI voxel, `status` is a flag with a nonzero-value for a tissue point, and `fibre_x, fibre_y, fibre_z` are x-, y- and z-components of the fibre orientation vector at that point. To reduce the size of the `.bbg` files, only the tissue points, that is points with nonzero `status` need to be specified, because the BeatBox solver will ignore the void points with zero status in any case. Although the original DT-MRI images data sets had $128 \times 128 \times 128$ voxels size, the actual dimensions of the foetal heart minimum bounding box were $67 \times 91 \times 128$, with 181070 tissue points.

The raw DT-MRI anatomy data (Pervolaraki et al., 2013) were segmented into the "tissue"/"not tissue" pixels discretion based on the MRI luminosity threshold, with the Cartesian fiber angles at each voxel obtained from the diffusion-weighted DT-MRI images. Only this basic segmentaion of the raw DT-MRI anatomy data (Pervolaraki et al., 2013) was taken into account in the computer simulation of cardiac re-entry dynamics, so we shall refer to it as the raw DT-MRI based anatomy model.

Any raw MRI and micro-CT image data show tiny bits of the preparation tissue, which usually get into the image together with the heart at the preparation stage. In the case of the raw DT-MRI image of the foetal heart (Pervolaraki et al., 2013), there happened to be a tiny bit of tissue at the bottom of the MRI image, adjacent to the apex of the foetal heart, see Figure 1, and the original Figure 2(a), last panel, in (Pervolaraki et al., 2013, p. 3). In order to see whether this tiny "leftover" piece of the heart tissue is capable to affect the outcome of a re-entry simulation, we edited the MRI images in order to remove the "leftover" piece, and then considered a comparison of the re-entry simulation in the two 3D DT-MRI based heart models: i) raw DT-MRI based anatomy model, and ii) "edited" DT-MRI based anatomy model without the tiny "leftover" piece of the heart tissue.

In case of the 2D model of a slice of the heart, in order to construct the 2D diffusivity tensor, the fibres vectors were projected into the plane of the slice of the heart.

2.3 Cardiac tissue model

To investigate the effects of anatomy on cardiac re-entry dynamics we used *monodomain* tissue model with non-flux boundary conditions

$$\frac{\partial \mathbf{u}}{\partial t} = \mathbf{f}(\mathbf{u}) + \nabla \cdot \hat{\mathbf{D}} \nabla \mathbf{u}, \qquad \vec{n} \cdot \hat{\mathbf{D}} \nabla \mathbf{u}\Big|_G = 0, \tag{1}$$

where $\mathbf{u}(\vec{r},t) = (u,v)^T$, $\vec{r}$ is the position vector, $\mathbf{f}(\vec{r},t) = (f,g)^T$ is the FitzHugh-Nagumo (Winfree, 1991) kinetics column-vector

$$\begin{aligned} f(u,v) &= \alpha^{-1}(u - u^3/3 - v), \\ g(u,v) &= \alpha\,(u + \beta - \gamma v), \end{aligned} \tag{2}$$

with the parameter values $\alpha = 0.3$, $\beta = 0.71$, $\gamma = 0.5$, which in an infinite excitable medium support a rigidly rotating vortex with positive filament tension (Biktashev et al., 1994). The simplified FHN model was intentionally chosen for this study in order to fully eliminate the possible effects of a realistic cell excitation kinetics, such as *e.g.* meander (Winfree, 1991), alternans (Karma, 1994), negative filament tension (Biktashev et al., 1994), etc., and in order to enhance and highlight the pure effects of the heart anatomy and anisotropy on the cardiac re-entry outcome. $\hat{\mathbf{D}} = \mathbf{Q}\hat{P}$, where $\mathbf{Q} = \mathrm{diag}(1,0) = \begin{bmatrix} 1 & 0 \\ 0 & 0 \end{bmatrix}$ is the matrix of the relative diffusion coefficients for u and v components, and $\hat{P} = [P_{jk}] \in \mathbb{R}^{3\times 3}$ is the u component diffusion tensor, which has only two different eigenvalues: the bigger, simple eigenvalue $P_\parallel$ corresponding to the direction along the tissue fibers, and the smaller, double eigenvalue $P_\perp$, corresponding to the directions across the fibres, so that

$$P_{jk} = P_\perp \delta_{jk} + \left(P_\parallel - P_\perp\right) f_j f_k, \tag{3}$$

where $\vec{f} = (f_k)$ is the unit vector of the fiber direction; $\vec{n}$ is the vector normal to the tissue boundary G. In the isotropic simulation, $P_\parallel$ and $P_\perp$ values were fixed at $P_\parallel = P_\perp = 1$ (corresponding 1D conduction velocity 1.89, in the dimensionless units of Eqs. (1)-(2)). In the anisotropic simulations, $P_\parallel$ and $P_\perp$ values were fixed at $P_\parallel = 2$, $P_\perp = 0.5$ (corresponding conduction velocities 2.68 and 1.34 respectively). All the conduction velocities have been computed for the period waves with the frequency of the free spiral wave in the model, i.e. 11.36. With the isotropic diffusivity ($P_\parallel = P_\perp = 1$) equal to the geometric mean between the faster and the slower anisotropic diffusivities ($P_\parallel = 2, P_\perp = 1/2$), the isotropic conduction velocity 1.89 was almost exactly the same as the geometric mean ≈ 1.895 of the faster and slower (2.68 and 1.34 respectively) anisotropic conduction velocities, chosen in order to minimize the maximal relative difference between the isotropic and anisotropic propagation speeds.

All the computer simulations presented here were done using the BeatBox (Antonioletti et al., 2017) software package with the explicit time-step Euler scheme, on the Cartesian regular grid with space step discretization $\Delta x = 0.1$, time step discretisation $\Delta t = 0.001$; 5-point stencil for isotropic, and 9-point stencil for anisotropic Laplacian approximation in 2D simulations; 7-point stencil for isotropic, and 27-point stencil for anisotropic Laplacian approximation in 3D simulations. The re-entry was initiated by the phase distribution method (Biktashev and Holden, 1998): in the 2D simulations, at a prescribed location of

the cross section of the DT-MRI based anatomical model shown in Figure 1; in the 3D simulations, at a prescribed location of the full DT-MRI based whole heart anatomical model.

The FHN model Eqs. (1)-(2) is not biophysically detailed and is formulated in dimensionless units. So, for illustrative purposes only, if we took the FHN time unit to be $1\,\mathrm{t.u.} = 40\,\mathrm{ms}$ this would give the APD90 of $125.6\,\mathrm{ms}$ which is within the range reported e.g. by (Zhu et al., 2016). The spiral wave period is then $454\,\mathrm{ms}$: at our chosen kinetics parameters, the spirals in FHN model have a big core. With the space step discretization $\Delta x = 0.1$ in FHN simulations, whereas the real grid resolution is $100\,\mu\mathrm{m} = 0.1\,\mathrm{mm}$, hence we would have the FHN space unit $1\,\mathrm{s.u.} = 1\,\mathrm{mm}$. The (geometric mean) diffusivity of $1\,\mathrm{s.u.}^2/\mathrm{t.u.}$ therefore works out as $0.025\,\mathrm{mm}^2/\mathrm{ms}$, and the corresponding conduction velocity of $1.89\,\mathrm{s.u.}/\mathrm{t.u.}$ is $0.04725\,\mathrm{mm}/\mathrm{ms}$. That gives a spiral wavelength of $\approx 21.45mm$. The conduction velocity thus obtained is within the range reported in (Pervolaraki et al., 2013), whereas the diffusivity is about four times smaller than the one used in (Pervolaraki et al., 2014). We must stress here that, since the FHN kinetics is not biophysically detailed, one should not expect anything more than an order-of-magnitude correspondence with reality.

3 RESULTS

3.1 2D MRI-based "slice" simulations

In the 2D simulations, Figure 2, a counter-clockwise re-entry was initiated by the phase distribution method (Biktashev and Holden, 1998), with the initial center of rotation placed at the prescribed location $x_0 = 40, y_0 = 60$ in the 2D cross section of the DT-MRI based anatomical model shown in Figure 1.

In the Figure 2(a-b), it can be seen that in both isotropic and anisotropic 2D simulations, at $t = 0$, there was identical location of the initial re-entry rotation center: roughly in the middle of the slice, in the vicinity of the septum cuneiform opening.

Figure 2(a) shows *isotropic* dynamics of the re-entry, that is with the fiber orientation data "turned OFF", so that only the geometry of the isotropic homogeneous slice affects the re-entry. While in an infinite medium the chosen FHN parameter values $\alpha = 0.3$, $\beta = 0.71$, $\gamma = 0.5$ produce rigidly rotating spiral (Winfree, 1991), the boundaries of the foetal heart slice model cause the drift of the re-entry. The re-entry does not terminate because of the reflection from the inexcitable boundaries (Biktashev and Holden, 1994), but after the transient first rotation around the septum cuneiform opening, the tip of the re-entry firmly pins (at $t = 35$) to the sharp lower end of the cuneiform opening, see Figure 2(a).

Figure 2(b) shows *anisotropic* dynamics of the re-entry, that is with the fiber orientation data "turned ON", so that both the geometry and the anisotropy of the otherwise homogeneous slice of the heart affect the dynamics of the re-entry, causing its drift. In the anisotropic slice, the re-entry also does not terminate at the inexcitable boundaries, but after a faster than in the previous isotropic case transient, compare the time units labels in the Figs. 2(a-b), the anisotropy of the medium turns the initial spiral wave into the fast anatomical re-entry around the septum cuneiform opening, see Figure 2(b).

3.2 3D whole heart MRI-based simulations

3.2.1 Raw DT-MRI anatomy model

In the 3D whole heart *raw* DT-MRI based simulations shown in the Figure 3 and Figure 4, a counter-clockwise excitation vortex was initiated by the phase distribution method (Biktashev and Holden, 1998), with the initial position of the transmural vortex filament (yellow line) at the prescribed location *along the*

194 x *axis* at $y_0 = 40, z_0 = 60$. It can be seen in Figure 3 isotropic, and Figure 4 anisotropic 3D simulations
195 that, at $t = 0$, there was identical initial location of the filament of the excitation vortex: that is transmurally,
196 roughly in the middle through the ventricles of the heart.

197 Figure 3 shows the *isotropic dynamics* of the excitation vortex, that is with the fiber orientation data
198 "turned OFF", so that only the geometry of the otherwise isotropic homogeneous foetal heart affects
199 dynamics of the vortex. At the chosen parameter values $\alpha = 0.3$, $\beta = 0.71$, $\gamma = 0.5$, the FHN vortex has
200 positive filament tension (Biktashev et al., 1994), and, depending on topology of an isotropic homogeneous
201 medium, either collapses or straightens up between parallell boundaries. In the isotropic simulations of
202 the foetal heart, boundaries of the heart cause the vortex to drift and collapse. However, there exist initial
203 locations of the excitation vortex, which although result in the drift of the vortex, still do not lead to the
204 expected collapse of the vortex with positive filament tension. One of such outcomes is shown in the
205 Figure 3. Here, following the geometry of the heart, after a very short transient, the initial vortex filament
206 breaks into the two major pieces, each of which finds its own synchronous pathway in the "isotropic"
207 foetal heart, resulting in the seemingly perpetual cardiac re-entry, which failed to self-terminate within the
208 extended simulation time $t = 30$. The time course of the instant number of filaments (blue dashed line) is
209 shown in Figure 12(a), and the time course of the instant total length of the filaments (blue dashed line)
210 is shown in Figure 12(b). It can be seen that, after a very fast transient increase in both the number of
211 filaments and the total length of the filaments, these fail to disappear, and keep oscilating around above zero
212 constants. The maximum instant number of the filaments in the simualtion was 9 at $t = 1.0$, the maximum
213 instant total length of the filaments was 127.1 at $t = 1.6$; while the time average number of the filaments in
214 the simualtion was 3.4, and the time average toatl length of the filaments was 29.3, see the summary of the
215 simulation detail in Figure 11.

216 Figure 4 shows *anisotropic dynamics* of the excitation vortex, that is with the fiber orientation data "turned
217 ON", so that both the geometry and the anisotropy of the otherwise homogeneous model of the foetal
218 heart affect dynamics of the vortex. Here, the anisotropy of the heart causes fast transient distortion of the
219 filament, and drift towards the inexcitable boundary of the heart, followed by the very fast self-termination
220 of the vortex by $t = 5.3$. The time course of the instant number of filaments (pink dotted line) is shown in
221 Figure 12(a), and the time course of the instant total length of the filaments (pink dotted line) is shown in
222 Figure 12(b). It can be seen that, after a very fast transient increase in both the number of the filaments
223 and the total length of the filaments, all the filaments rapidly disappear. The maximum instant number of
224 the filaments was 13 at $t = 0.8$, that is higher and achieved faster than in the isotropic conduction. The
225 maximum instant total length of the filaments was 179.7 at $t = 1.8$, again much higher than in the isotropic
226 conduction. The time average number of the filaments in the simualtion was 6.5, twice higher than in the
227 isotropic conduction, and the time average total length of the filaments was 91.2, three times higher than in
228 the isotropic conduction, see the summary of the simulation detail in Figure 11.

229 In the 3D whole heart *raw* DT-MRI based simulations shown in the Figure 5 and Figure 6, a counter-
230 clockwise excitation vortex was initiated by the phase distribution method (Biktashev and Holden, 1998),
231 with the initial position of the transmural vortex filament (yellow line) at the prescribed location *along the*
232 y *axis* at $x_0 = 40, z_0 = 60$, that is *perpendicular* to the initial orientation of the vortex filament shown in
233 Figure 3 and Figure 4. It can be seen in Figure 5 isotropic, and in Figure 6 anisotropic 3D simulations, that
234 at $t = 0$, there was identical intial location of the filament of the excitation vortex: that is transmurally,
235 roughly in the middle through the ventricles of the foetal heart, and *perpendicular* to the initial orientation
236 of the vortex filament shown in Figure 3 and Figure 4.

Figure 5 shows the *isotropic dynamics* of the excitation vortex, that is with the fiber orientation data "turned OFF", so that only the geometry of the otherwise isotropic homogeneous foetal heart affects dynamics of the vortex. Here, contrary to the expectation for the positive filament tension vortex to always contract, the organising filament first transiently extends intramurally along the tissue walls, before the final break up into the two ring-like pieces, each of which then quickly contracts and terminates at the opposite base and apex regions of the heart by $t = 4$. The time course of the instant number of filaments (blue dashed line) is shown in Figure 12(c), and the time course of the instant total length of the filaments (blue dashed line) is shown in Figure 12(d). It can be seen that, after a very fast transient increase in both the number of the filaments and the total length of the filaments, all the filaments rapidly disappear. The maximum instant number of the filaments was 12 at $t = 1.4$, with the maximum instant total length of the filaments 188.0 achieved at $t = 1.5$. The time average number of the filaments in the simualtion was 4.7, and the time average total length of the filaments was 80.5, see the summary of the simulation detail in Figure 11. It can be seen that in this isotropic conduction simulation, with just a different location/orientation of the initial vortex filament, the time average total length of the vortex filaments was two and a half times higher than in the failed to self-terminate isotropic conduction simulation shown in Figure 3.

Figure 6 shows *anisotropic dynamics* of the excitation vortex, that is with the fiber orientation data "turned ON", so that both the geometry and the anisotropy of the otherwise homogeneous model of the heart affect dynamics of the vortex leading to its really fast termination at the apex of the heart by $t = 2.6$. The time course of the instant number of filaments (pink dotted line) is shown in Figure 12(c), and the time course of the instant total length of the filaments (pink dotted line) is shown in Figure 12(d). It can be seen that, after a very fast transient increase in both the number of the filaments and the total length of the filaments, all the filaments rapidly disappear. The maximum instant number of the filaments was 17 at $t = 0.5$, that is higher and achieved faster than in the corresponding isotropic conduction shown in Figure 5. The maximum instant total length of the filaments was 278.6 at $t = 0.9$, again much higher than in the corresponding isotropic conduction. The time average number of the filaments in the simualtion was 9.5, twice higher than in the isotropic conduction, and the time average total length of the filaments was 152.6, also twice higher than in the isotropic conduction, see the summary of the simulation detail in Figure 11.

It can be seen in the *raw* DT-MRI model simulations shown in Figure 3, Figure 4, Figure 5, and Figure 6, that although the organising filament of the vortex could not get through into the accidental "leftover" piece of tissue adjacent to the apical region, the piece still got activated, and could have served as an artificial "capacitor" affecting dynamics of the re-entry. In order to check whether this might be the case, we edited the original raw DT-MRI model by removing in the MRI the foreign "leftover" piece, and repeated the whole heart isotropic and anisotropic simulations from the same two orthogonal initial locations of the re-entry, similar to the shown in Figure 3, Figure 4, Figure 5, and Figure 6.

3.2.2 "Edited" DT-MRI anatomy model

In the 3D whole heart *"edited"* MRI model simulations shown in the Figure 7 and Figure 8, a counter-clockwise excitation vortex was initiated by the phase distribution method (Biktashev and Holden, 1998), with the initial position of the transmural vortex filament (yellow line) at the prescribed location *along the* x *axis* at $y_0 = 40, z_0 = 60$. It can be seen in Figure 7 isotropic, and in Figure 8 anisotropic 3D simulations, that, at $t = 0$, there was identical initial location of the filament of the excitation vortex: that is transmurally, roughly in the middle through the ventricles of the foetal heart, similar to the initial location of the vortex filament in the raw DT-MRI simulations shown in Figure 3 and Figure 4 .

Figure 7 shows *isotropic dynamics* of the vortex, that is with the fiber orientation data "turned OFF", so that only the geometry of the otherwise isotropic homogeneous foetal heart affects dynamics of the vortex. Here, following the geometry of the heart, the initial filament also breaks into the two major pieces, each of which also finds its own synchronous pathway similar to the beginning of the raw DT-MRI simulation shown in Figure 3. However, this time, after just a few rotations, the two re-entries find their end in their almost synchronous termination in the base region of the heart by $t = 16.9$. The time course of the instant number of filaments (green dashed line) is shown in Figure 12(a), and the time course of the instant total length of the filaments (green dashed line) is shown in Figure 12(b). It can be seen that, after a very fast transient increase in both the number of the filaments and the total length of the filaments, all the filaments rapidly disappear. The maximum instant number of the filaments was 9 at $t = 0.2$. The maximum instant total length of the filaments was 122.3 at $t = 0.7$. The time average number of the filaments in the simualtion was 3.2, and the time average total length of the filaments was 28.7, see the summary of the simulation detail in Figure 11. It can be seen that, in the "edited" MRI isotropic simulation in Figure 7, the maximum instant and the time average number of the filaments, as well as the maximum instant and the time average total length of the filaments, were practically the same as in the corresponding raw MRI isotropic simulation with the failed to self-terminate re-entry shown in Figure 3. The only quantitative difference between the two isotropic simulations, *i.e.* the perpetual re-entry in Figure 3 *vs* the self-termination in Figure 7, was that, in the "edited" MRI isotropic simulation, without the "leftover" piece of tissue adjacent to the apex of the heart, the maximum instant number of the filaments, and the maximum instant total length of the filaments were achieved much faster: by $t = 0.2$ and $t = 0.7$ correspondingly.

Figure 8 shows *anisotropic dynamics* of the vortex, that is with the fiber orientation data "turned ON", so that both the geometry and the anisotropy of the otherwise homogeneous model of the heart affect dynamics of the vortex. Here, the anisotropy of the heart also causes significant transient distortion of the initial filament, followed by the fast drift towards the apex, with the ultimate termination at the AV border before a completion of a single rotation, very similar to the corresponding raw DT-MRI anisotropic simulation shown in Figure 4. However, in the "edited" MRI model without the "leftover" piece adjacent to the apex, repolarisation of the heart is faster than it was in the presence of the "incidental capacitor" effect in the corresponding raw DT-MRI simulation shown in Figure 4. The time course of the instant number of filaments (red solid line) is shown in Figure 12(a), and the time course of the instant total length of the filaments (red solid line) is shown in Figure 12(b). It can be seen that, after a very fast transient increase in both the number of the filaments and the total length of the filaments, all the filaments rapidly disappear by $t = 4.8$. The maximum instant number of the filaments was 17 at $t = 0.4$, that is higher than in the corresponding raw anisotropic conduction shown in Figure 4, and twice higher than in the corresponding "edited" isotropic conduction shown in Figure 7. The maximum instant total length of the filaments was 180.3 at $t = 0.7$, similar to the corresponding raw anisotropic conduction shown in Figure 4, and much higher than in the corresponding "edited" isotropic conduction shown in Figure 7. The time average number of the filaments in the simualtion was 6.3, similar to the corresponding raw anisotropic conduction shown in Figure 4, and twice higher than in the corresponding "edited" isotropic conduction shown in Figure 7. The time average total length of the filaments was 95.4, similar to the corresponding raw anisotropic conduction shown in Figure 4, and three times higher than in the corresponding raw isotropic conduction shown in Figure 4. Time to the maximum number of the filaments ($t = 0.4$), and time to the maximum total length of the filaments ($t = 0.7$), were similar to the corresponding "edited" isotropic conduction shown in Figure 7, and twice faster than in the corresponding raw anisotropic conduction shown in Figure 4, see the summary of the simulation detail in Figure 11. So, that the anisotropy of the heart increased the number and the total

length of the filaments, and shortened the time to self-termination by folds, while the "incidental capacitor" effect of the "leftover" piece adjacent to the apex slowed down the process.

In the 3D whole heart *"edited"* MRI simulations shown in Figure 9 and Figure 10, a counter-clockwise excitation vortex was initiated by the phase distribution method (Biktashev and Holden, 1998), with the initial position of the transmural filament (yellow line) at the prescribed location *along the* y *axis* at $x_0 = 40, z_0 = 60$. It can be seen in Figure 9 isotropic, and in Figure 10 anisotropic 3D simulations, that at $t = 0$, there was the identical initial location of the filament: that is transmurally, roughly in the middle through the ventricles of the heart, perpendicular to the filament initial location in the "edited" MRI simulations shown in Figure 7 and Figure 8, and similar to the initial location of the filament in the raw DT-MRI simulations shown in Figure 5 and Figure 6 .

Figure 9 shows "edited" MRI *isotropic dynamics* of the vortex, that is with the fiber orientation data "turned OFF", so that only the geometry of the otherwise isotropic homogeneous foetal heart affects the vortex. Here, again contrary to the expectation for a positive filament tension vortex to always contract, the organising filament first transiently extends intramurally before breaking up into the two ring-like pieces, each of which quickly contracts and terminates at the opposite base and apex regions of the heart, identical to what was seen in the raw DT-MRI simulation shown in Figure 5. The time course of the instant number of filaments (green dashed line) is shown in Figure 12(c), and the time course of the instant total length of the filaments (green dashed line) is shown in Figure 12(d). It can be seen that, after a very fast transient increase both in the number of the filaments and in the total length of the filaments, all the filaments rapidly disappear by $t = 4.0$. The maximum instant number of the filaments was 12 at $t = 0.5$. The maximum instant total length of the filaments was 190.7 at $t = 1.5$. The time average number of the filaments in the simualtion was 4.7, and the time average total length of the filaments was 82.9, see the summary of the simulation detail in Figure 11. So, from the comparison with the corresponding raw MRI isotropic simulaton shown in Figure 5, it seems that, for that particular initial location of the filament, the "leftover" tissue did not play any role in the re-entry self-termination time.

Figure 10 shows *anisotropic dynamics* of the vortex, that is with the fiber orientation data "turned ON", so that both the geometry and the anisotropy of the otherwise homogeneous model of the heart affect the vortex, which, in the absence of the "incidental capacitor" effect of the "leftover" piece, results in the fastest possible termination of the re-entry at the apex of the heart by $t = 2.3$, before the vortex first rotation ever started. The re-entry termination time here is more than twice shorter than in both the raw MRI isotropic simulation shown in Figure 5, and in the "edited" isotropic simulations shown in Figure 9; shorter than in the corresponding simulation with the "incidental capacitor" effect shown in the Figure 6, and times shorter than in any of the simulations of the re-entry with the perpendicular initial location of the filament shown in the Figure 3, Figure 4, Figure 7, and Figure 8 . So, that the main reasons for the re-entry fastest self-termination seem to be the initial location of the filament and the anisotropy of the heart.

In Figure 11, we have summarized the results of the *raw* MRI simulations shown in Figure 3, Figure 4, Figure 5, Figure 6, and the *"edited"* MRI simulations shown in Figure 7, Figure 8, Figure 9, and Figure 10. The re-entry termination time, in the time units of Eqs. (1)-(2), is shown under each respected whole heart model initiation cite panel. It can be seen that the anisotropy of the heart causes at least twice faster termination of re-entry. It also can be seen that indeed the "leftover" piece of tissue connected to the apical region of the heart in the raw DT-MRI model served as an artificial "capacitor" affecting the re-entry dynamics, and significantly prolongated the life time of re-entry initiated at the particular location/orientation respective to the "capacitor".

Finally, the 3D anatomically realistic simulations of the foetal heart show that the anisotropy of the heart causes the fast transient increase in the number and the total length of the filaments, see Figure 12, with the typical fast drift towards the apex area of the heart, and re-entry self-termination, see also the movies in the Supplementary Material section 5.1.

4 DISCUSSION

Although the role of heart anatomy and anisotropy in the origin and sustainability of cardiac arrhythmias has been appreciated for a long time, there is limited experimental evidence to clarify detail of the heart anatomy effect on persistent cardiac arrhythmias and fibrillation. In particular, the theoretically plausible hypothesis that the anisotropic discontinuities in the heart might be a source of rise for cardiac re-entry due to the abrupt change in conduction velocity and wavefront curvature (Fenton and Karma, 1998; Spach, 2001; Smaill et al., 2004) was in controversy with the observation that the transmural fiber arrangement, including the range of transmural change in fiber angle in ventricular wall, although varied between species (Hunter et al., 1997, p. 173), was consistent within a species. So that the question was that, if the pro-arrhythmic mechanism of cardiac re-entry initiation by the anisotropic discontinuities in a heart (Fenton and Karma, 1998; Spach, 2001; Smaill et al., 2004) was correct, what would then have been a reason for the consistent structure (Hunter et al., 1997, p. 173) of the anisotropic discontinuities in healthy mammalian hearts. The combination of the High Performance Computing with the high-resolution DT-MRI based anatomy models of the heart allows anatomically realistic *in-silico* testing of the effects of individual heart anatomy and anisotropy on the cardiac re-entry dynamics (Vigmond et al., 2009; Bishop et al., 2010; Kharche et al., 2015a,b; Antonioletti et al., 2017). In this paper, for the first time, we present the anatomy and myofiber structure realistic computer simulation study of the cardiac re-entry dynamics in the DT-MRI based model of the human foetal heart (Pervolaraki et al., 2013).

The human foetal heart single anisotropic geometry dataset used in these simulations needs to be a typical and accurate representation of the cardiac structure and tissue architecture, with a spatial resolution suitable for numerical solution of the excitation equations. For a smoothly changing anisotropic geometry the imaged dataset may be interpolated to provide sufficient spatial resolution. DT-MRI has provided 17 – 200 cubic voxel datasets of human foetal heart (Pervolaraki et al., 2012, 2013, 2017; Tang et al., 2016). Finite difference numerical solutions of propagation in biophysically detailed models of adult cardiac tissue need $\sim 100\mu m$ space steps in a Cartesian coordinate system. During foetal development the structure of the heart changes, the ventricular wall is compactified and trabeculated, and the size of the heart increases. Any atlas of the developing human foetal heart would need to come from longitudinal studies (which are impractical and potentially unethical), or from a large number of hearts obtained and imaged at different gestational ages. Here, all simulations are done on a single cardiac geometry that was selected as the transmural changes in fiber helix angle had developed. The results illustrated are specific for this particular anisotropic cardiac geometry, which is critically determined by how it was imaged and reconstructed. The fiber orientation angles of the heart were obtained from the orientation of the DT-MRI primary eigenvectors. Propagation velocity was twice as fast along the fibres than across the fibers. In all the simulations on this DT-MRI based cardiac geometry, the anisotropy of the myocardial tissue shortens the duration of re-entry by several fold. The numerical simulations depend on the validity of the DT-MRI dataset used. The ventricular wall showed the characteristic transmural rotation of the helix angle of the developed mammalian heart, while the fiber orientation in the atria was irregular. We expect the results be subsequently verified on other anatomy data, including different technique data e.g. MRI vs DT-MRI vs micro-CT vs serial section histology, etc.

The comparative isotropic *vs* anisotropic simulation of the otherwise homogeneous model of the foetal heart shows that, in the 2D slice of the heart, the fiber anisotropy might change the re-entry dynamics from the re-entry pinned at the sharp end of the septum cuneiform opening, Figure 2(a), into the fast anatomical re-entry around the opening, Figure 2(b). Note that, despite of the only basic segmentation of the MRI model into the tissue/not tissue points, and the ventricles not being isolated from the atria, because of the 2D re-entry pinning to either the sharp end of the septum opening, as in the isotropic simulation shown in Figure 2(a), or to the whole septum opening, as in the case of anatomical re-entry in the anisotropic simulation shown in Figure 2(b), the tip of the re-entry never penetrated from the ventricles into the atria.

Although, from the cardiac physiology point of view, the only basic segmentation of the raw DT-MRI data (Pervolaraki et al., 2013) into the tissue/non-tissue pixels might be seen as a major limitation of the study, from the non-linear science point of view, the use of the raw MRI data, as an example of a nature provided medium to study a re-entry dynamics, gives an important insight into the pure anatomy induced drift in an otherwise homogeneous 2D medium, and into the possibility of pinning of the re-entry not to a major blood vessel but to a sharp end of an anatomical openning (Biktasheva et al., 2015); and into that a real fiber anisotropy is capable to turn the pinned re-entry into an anatomical one. Importantly though, the 2D simulations in Figure 2 are an important step to highlight the role and the necessity of the whole heart structure in the re-entry dynamics and self-termination.

In the 3D DT-MRI based *isotropic* model of the foetal heart, depending on the initial location/orientation of the re-entry organising filament, the geometry of the foetal heart might sustain perpetual cardiac re-entry even with a positive filament tension, see Figure 3 and Figure 12(a-b). However, if the same positive filament tension vortex is initiated at the exactly same location/orientation in the *anisotropic* DT-MRI based model, the fiber structure of the foetal heart facilitates fast self-termination of cardiac re-entry, see Figure 4 and Figure 12(a-b).

From the respective comparison of the "isotropic *vs* anisotropic" simulations in Figure 3 *vs* Figure 4, and Figure 7 *vs* Figure 8, it can be seen that, whereas the re-entry organizing filaments were capable to penetrate from the ventricles to atria in the isotropic simulations shown in Figure 3 and Figure 7, the abrupt change in the fiber angles between the atria and the ventricles, which one can see in Figure 1, did not allow the organizing filaments to penetrate from ventricles into atria in the anisotropic simulations shown in Figure 4 and Figure 8, so that the anisotropy of ventricles could complete the speedy elimination of the re-entry within a single rotation.

The comparison of re-entry termination times in the whole heart raw DT-MRI simulations shown in Figure 3, Figure 4, Figure 5, and Figure 6, with the corresponding "edited" MRI simulations shown in Figure 7, Figure 8, Figure 9, and Figure 10, showed that, although the filament of cardiac re-entry never got through into the tiny piece of the "leftover" tissue adjacent to the apex of the heart in the raw DT-MRI , the "not heart" excitable tissue served as an accidental "capacitor", significantly prolongating the life time of cardiac re-entry initiated at a particular location/orientation respective to the "leftover" piece location/orientation. The comparison of the re-entry termination times in Figure 11 and Figure 12 shows that the higher maximum number of the filaments and the bigger total length of the filaments tend to correlate with the faster termination of re-entry. However, the usual transient increase in both the number of the filaments and in the total length of the filaments, still failed to identify and terminate the persistent re-entry shown in Figure 3 and Figure 12(a-b).

The "isotropic *vs* anisotropic" comparison of self-termination time, both in the raw and in the "edited" MRI whole heart simulations, confirmed that, regardless of with or without the "leftover" piece adjacent

to the apex, anisotropy of the heart shortens re-entry self-termination time several folds, see Figure 11 and Figure 12. Figure 12 shows that anisotropy increases the maximum number and the maximum total length of the filaments. The bigger maximum number and the maximum total length of the filaments tend to correlate with the faster termination of re-entry. The biggest transient total lengths of the filaments was in the anisotropic case of re-entry initiated *along the y axis*, see the corresponding dotted pink and solid red lines in panel **(d)** in Figure 12, which ensured the re-entry fastest termination. It can be seen from Figure 5, Figure 6, Figure 9, and Figure 10, that the initial position of the filament *along the y axis* allowed the filament to grow intramurally, thus maximally increasing the transient total length of the filaments, and shortenning their termination time.

The comparison of the "edited" MRI simulations of thus completely isolated heart shown in Figure 7, Figure 8, Figure 9, and Figure 10, with the raw DT-MRI simulations shown in Figure 3, Figure 4, Figure 5, Figure 6, provide an important new insight into cardiac re-entry dynamics. Namely, that an excitable tissue accidentally adjacent to the heart might serve a capacitor capable to extend re-entry self-termination time, see for the respective comparison Figure 3 *vs* Figure 7, Figure 4 *vs* Figure 8, Figure 5 *vs* Figure 9, and Figure 6 *vs* Figure 10, summarised in Figure 11 and Figure 12. The latter suggests a possible new mechanism for a persistent cardiac re-entry. That is if, apart from the major blood vessels normally adjacent to the heart in vivo, and affecting cardiac re-entry dynamics, there were also an accidental "touching" of the heart by an adjacent excitable tissue, for example, due to a change of posture in the night (Hu et al., 2011), the "incidental capacitor" effect could have extended re-entry self-termination time, up to the failure to self-terminate. The "incidental capacitor" hypothesis could be an additional explanation to the circadian rhythm (Jeyaraj et al., 2012), for the elusive and difficult to reporduce longer arrhythmia episodes reported in the night ECGs as opposed to the on average shorter arrhythmias in the day time ECGs. Although the raw DT-MRI simulations with the "leftover" piece of tissue might have been seen a limitation of the study, the real heart in vivo does not exist in complete isolation from the main blood vessels and other neighboring tissues. So, we believe that our "incidental" leftover tissue results only once more confirm the importance and the necessity of taking into account of the real anatomical settings and surrounding of the heart for the full appreciation of cardiac re-entry dynamics.

The BeatBox DT-MRI based *in-silico* comparative study confirms the heart anatomy and anisotropy functional effect on cardiac re-entry self-termination as opposed to its sustainability, pinning to anatomical features, transformation from pinned to anatomical re-entry, while the anisotropy of the tissue facilitates re-entry self-termination.

One of the limitations of the present study is the use of the simplified FitzHugh-Nagumo (Winfree, 1991) excitation model, chosen for this study in order to eliminate the effects of realistic cell excitation kinetics, such as *e.g.* meander (Winfree, 1991), alternans (Karma, 1994), negative filament tension (Biktashev et al., 1994), etc., and enhance and highlight the pure effects of the heart anatomy and anisotropy on the re-entry. The realistic cell excitation models should be used in the future studies, in order to clarify specific interplay of the cell kinetics with the heart anatomy and anisotropy.

As it can be seen from Figure 1 (for the color-encoded fractional anisotropy (FA) and for the color-encoded all the three components of the fiber angles see also Figure 4 in (Pervolaraki et al., 2013, p. 5)), formation of the foetal heart fiber structure at the epicardium and endocardium is not completed yet, so that only the already formed intramural laminar myofibers affect dynamics of the re-entry. Although the use of the not fully formed foetal heart can be seen as a limitation of the study, on the other hand, the irregular epicardium and endocardium fibers seem to prevent a re-entry from pinning to the fine endocardium features, which were yet to be developed (Pervolaraki et al., 2013) later on. We appreciate

that the anatomy and fiber structure differences in the foetal and in a fully formed adult heart might alter the re-entry dynamics, such as in *e.g.* the reported case of re-entry pinning to the junction of pectinate muscles with crystae terminalis in adult human atrium (Wu et al., 1998; Yamazaki et al., 2012; Kharche et al., 2015a). That is, although it is possible to initiate a cardiac re-entry in the tiny $1.4g$ (at 143 DGA) foetal heart (Pervolaraki et al., 2013), the already formed intramural laminar anisotropy of the foetal heart facilitates the re-entry self-termination, Figure 11. With the hindsight of the present study, in an adult heart, because of the pinning opportunities provided by the endocardium anatomical features (Wu et al., 1998; Yamazaki et al., 2012; Kharche et al., 2015a), there must exist additional mechanisms to facilitate cardiac re-entry self-termination (Clayton et al., 1993).

The most serious limitation of the study is that only the basic segmentation of the raw DT-MRI data (Pervolaraki et al., 2013) into the tissue/non-tissue pixels based on the MRI luminosity threshold, and only the primary eigenvalues of fibres orientation, were taken into account in the BeatBox (Antonioletti et al., 2017) computer simulations of cardiac re-entry dynamics. Further levels of DT-MRI segmentation, in order to take into account e.g. the heart collagen skeleton, isolation of ventricles from atria, etc., will inevitably change the outcome of the re-entry, by adding the electrically impermeable barriers to cardiac re-entry. Currently, this further segmentation is added into DT-MRI based models via complex rule based image post-processing (Lombaert et al., 2012; Gahm et al., 2013), which brings in artificial assumptions, as well as limits the number of available segmented data sets. From the non-linear science point of view we pursued in this initial study, the rationale was to use the raw DT-MRI as an example of a nature provided medium to study a re-entry dynamics. In the future, the multichannel computer tomography might offer automatic tissue segmentation, so that multi-level segmented DT-MRI based models become more available, and be used in the BeatBox (Antonioletti et al., 2017) anatomically and biophysically realistic simulations.

Finally, we believe that a simple "mechanistic" explanation, although often craved for, might be rather inadequate/premature here, and will require better theoretical understanding of the demonstrated potential effect of the heart anatomy and anisotropy on cardiac re-entry dynamics, for it is not a particular feature, or a sequence of features, but rather the whole complex of the shape, anisotropy, and position of the heart within the body, which affects the re-entry dynamics in a particular way, and which seems to have evolved in order to ensure the fastest self-termination of cardiac re-entry. If our hypothesis is correct, it might explain the difficulties with reproducibility of the arrhythmia in vivo and in an isolated heart. A general role of fiber anisotropy in the genesis and sustenance of arrhythmias could be and has been addressed by numerics on idealised and simplified geometries with different spatial distributions of anisotropy (Fenton and Karma, 1998). The biomedical question addressed in the manuscript is whether self-terminating ventricular arrhythmias can occur in a developing foetal heart, as has inferred from fECG data in (Benson et al., 2015). The most important novel finding of the paper is that, contrary to what currently seems to be a commonly accepted view of the pro-arrhythmic nature of cardiac anisotropy, the point of view based on the mainly theoretical and simplified anatomy models studies, for the first time ever, and for the first time in a real whole heart DT-MRI based model, we have demonstrated that anisotropy of the heart might have rather anti-arrhythmic effect, as it facilitates the fastest self-termination of cardiac re-entry.

5 NOMENCLATURE

5.1 Resource Identification Initiative

BeatBox, RRID:SCR_015780

CONFLICT OF INTEREST STATEMENT

The authors declare that the research was conducted in the absence of any commercial or financial relationships that could be construed as a potential conflict of interest.

ETHICS STATEMENT

Tissue acquisition followed medical termination of pregnancy with written and informed consent, and Ethical approval from Lothian Research Ethics Committee (reference 08/S1101/1). Temporary storage of the tissue for imaging was in premises licensed under the UK 2004 Human Tissues Act.

AUTHOR CONTRIBUTIONS

IVB, AVH, EP and FCW contributed conception and design of the study; RAA, AVH and EP contributed the human foetal heart DT-MRI data sets; IVB and FCW converted the DT-MRI data sets into BeatBox geometry format and ran the simulations; IVB performed visualisation of the simulations and analysis, and wrote the first draft of the manuscript. FCW approved submission of the paper. IVB, RAA, AVH, and EP contributed to manuscript revision, read and approved the submitted version.

FUNDING

We acknowledge the support of the UK Medical Research Council grant G1100357 for the human foetal heart DT-MRI data sets. We also wish to acknowledge the support of the BeatBox software development project by EPSRC (UK) grants EP/I029664 and EP/P008690/1.

ACKNOWLEDGMENTS

We thank all the developers of the BeatBox HPC Simulation Environment for Biophysically and Anatomically Realistic Cardiac Electrophysiology. We are grateful to Professor V.N.Biktashev for much appreciated advice and discussion.

SUPPLEMENTARY MATERIAL

The Supplementary Material for this article can be found online at ...

REFERENCES

Allessie, M. A., Bonke, F. I. M., and Schopman, F. J. (1973). Circus movement in rabbit atrial muscle as a mechanism of tachycardia. *Circ. Res.* 32, 54–62

Anselmino, M., Blandino, A., Beninati, S., Rovera, C., Boffano, C., Belletti, M., et al. (2011). Morphologic analysis of left atrial anatomy by magnetic resonance angiography in patients with atrial fibrillation: a large single center experience. *Journal of Cardiovascular Electrophysiology* 22, 1–7

Antonioletti, M., Biktashev, V. N., Jackson, A., Kharche, S. R., Stary, T., and Biktasheva, I. V. (2017). Beatbox - hpc simulation environment for biophysically and anatomically realistic cardiac electrophysiology. *PLoS ONE* 12(5), e0172292. doi:https://doi.org/10.1371/journal.pone.0172292

Balakhovsky, I. (1965). Some regimes of excitation movement in an ideal excitable tissue. *Biofizika* 9, 1–63. In Russian

563 Benson, A., Hayes-Gill, B., Holden, A., Matthews, R., Naz, A., Page, S., et al. (2015). Self-terminating
564 re-entrant cardiac arrhythmias: quantitative characterization. *Computing in Cardiology* 42, 641–644
565 Biktashev, V. N. (1998). A three-dimensional autowave turbulence. *Int. J. of Bifurcation and Chaos* 8,
566 677–684
567 Biktashev, V. N., Barkley, D., and Biktasheva, I. V. (2010). Orbital motion of spiral waves in excitable
568 media. *Phys Rev Lett* 104, 058302
569 Biktashev, V. N., Biktasheva, I. V., and Sarvazyan, N. A. (2011). Evolution of spiral and scroll waves of
570 excitation in a mathematical model of ischaemic border zone. *PLoS ONE* 6, e24388
571 Biktashev, V. N. and Holden, A. (1998). Re-entrant waves and their elimination in a model of mammalian
572 ventricular tissue. *Chaos* 8, 48–56
573 Biktashev, V. N. and Holden, A. V. (1994). Design principles of a low-voltage cardiac defibrillator based
574 on the effect of feed-back resonant drift. *J. Theor. Biol.* 169, 101–113
575 Biktashev, V. N., Holden, A. V., and Zhang, H. (1994). Tension of organizing filaments of scroll waves.
576 *Phil. Trans. Roy. Soc. Lond. ser. A* 347, 611–630
577 Biktasheva, I. V. and Biktashev, V. N. (2003). Wave-particle dualism of spiral waves dynamics. *Phys. Rev.*
578 *E* 67, 026221
579 Biktasheva, I. V., Dierckx, H., and Biktashev, V. N. (2015). Drift of scroll waves in thin layers caused by
580 thickness features: asymptotic theory and numerical simulations. *Phys. Rev. Lett.* 114, 068302
581 Bishop, M. J. and Plank, G. (2012). The role of fine-scale anatomical structure in the dynamics of reentry in
582 computational models of the rabbit ventricles. *JOURNAL OF PHYSIOLOGY-LONDON* 590, 4515–4535
583 Bishop, M. J., Plank, G., Burton, R., Schneider, J., Gavaghan, D., Grau, V., et al. (2010). Development
584 of an anatomically detailed MRI-derived rabbit ventricular model and assessment of its impact on
585 simulations of electrophysiological function. *AMERICAN JOURNAL OF PHYSIOLOGY-HEART AND*
586 *CIRCULATORY PHYSIOLOGY* 298, H699–H718
587 Bishop, M. J., Vigmond, E., and Plank, G. (2011). Cardiac bidomain bath-loading effects during
588 arrhythmias: Interaction with anatomical heterogeneity. *Biophysical Journal* 101, 2871–2881
589 Bosch, R. F. and Nattel, S. (2002). Cellular electrophysiology of atrial fibrillation. *Cardiovascular*
590 *Research* 54, 259–269
591 Clayton, R., Murray, A., Higham, P., and Campbell, R. (1993). Self-terminating ventricular
592 tachyarrhythmias - a diagnostic dilemma. *LANCET* 341, 93–95
593 Davydov, V. A., Zykov, V. S., Mikhailov, A. S., and Brazhnik, P. K. (1988). Drift and resonance of spiral
594 waves in active media. *Radiofizika* 31, 574–582. In Russian
595 Dierckx, H., Brisard, E., Verschelde, H., and Panfilov, A. (2013). Drift laws for spiral waves on curved
596 anisotropic surfaces. *Phys. Rev. E* 88, 012908
597 Eckstein, J., Maesen, B., Linz, D., Zeemering, S., van Hunnik, A., Verheule, S., et al. (2011). Time
598 course and mechanisms of endo-epicardial electrical dissociation during atrial fibrillation in the goat.
599 *CARDIOVASCULAR RESEARCH* 89, 816–824
600 Eckstein, J., Zeemering, S., Linz, D., Maesen, B., Verheule, S., van Hunnik, A., et al. (2013).
601 Transmural conduction is the predominant mechanism of breakthrough during atrial fibrillation: Evidence
602 from simultaneous endo-epicardial high-density activation mapping. *Circulation: Arrhythmia and*
603 *Electrophysiology* 6, 334–341
604 Ermakova, E. A., Pertsov, A. M., and Shnol, E. E. (1989). On the interaction of vortices in 2-dimensional
605 active media. *Physica D* 40, 185–195
606 Fenton, F. and Karma, A. (1998). Vortex dynamics in three-dimensional continuous myocardium with fiber
607 rotation: Filament instability and fibrillation. *Chaos* 8, 20–47

608 Fukumoto, K., Habibi, M., Ipek, S., E. G. Zahid, Khurram, I. M., Zimmerman, S. L., Zipunnikov, V.,
609 et al. (2016). Association of left atrial local conduction velocity with late gadolinium enhancement on
610 cardiac magnetic resonance in patients with atrial fibrillation. *CIRCULATION-ARRHYTHMIA AND*
611 *ELECTROPHYSIOLOGY* 9, e002897
612 Gahm, J. K., Kung, G. L., and Ennis, D. B. (2013). Weighted component-based tensor distance applied to
613 graph-based segmentation of cardiac dt-mri. In *2013 IEEE 10TH INTERNATIONAL SYMPOSIUM ON*
614 *BIOMEDICAL IMAGING (ISBI)*. IEEE International Symposium on Biomedical Imaging, 504–507
615 Garey, W. E. (1914). The nature of fibrillatory contraction of the heart – its relation to tissue mass and
616 form. *Am. J. Physiol.* 33, 397–414
617 Gray, R. A., Pertsov, A. M., and Jalife, J. (1996). Incomplete reentry and epicardial breakthrough patterns
618 during atrial fibrillation in the sheep heart. *Circulation* 94, 2649–2661
619 Hu, K., Scheer, F., Laker, M., Smales, C., and Shea, S. (2011). Endogenous circadian rhythm in vasovagal
620 response to head-up tilt. *CIRCULATION* 123, 961–U85
621 Hunter, P. J., Smaill, B. H., Nielsen, P. M. F., and Le Grice, I. J. (1997). A mathematical model of cardiac
622 anatomy. In *Computational Biology of the Heart*, eds. A. V. Holden and A. V. Panfilov (Chichester:
623 Wiley), 171–215
624 Jeyaraj, D., Haldar, S., Wan, X., McCauley, M., Ripperger, J., Hu, K., et al. (2012). Circadian rhythms
625 govern cardiac repolarization and arrhythmogenesis. *NATURE* 483, 96–U141. doi:10.1038/nature10852
626 Karma, A. (1994). Electrical alternans and spiral wave breakup in cardiac tissue. *CHAOS* 4, 461–472
627 Keener, J. P. (1988). The dynamics of three-dimensionsional scroll waves in excitable media. *Physica D*
628 31, 269–276
629 Kharche, S. R., Biktasheva, I. V., Seeman, G., Zhang, H., and Biktashev, V. N. (2015a). A computer
630 simulation study of anatomy induced drift of spiral waves in the human atrium. *BioMed Research*
631 *International* 2015, 731386
632 Kharche, S. R., Biktasheva, I. V., Seemann, G., Zhang, H., Zhao, J., and Biktashev, V. N. (2015b).
633 Computational modelling of low voltage resonant drift of scroll waves in the realistic human atria.
634 *Lecture Notes in Computer Science* 9126, 421–429
635 Krinsky, V. (1968). Fibrillation in the excitable media. *Problemy Kibernetiki* 2, 59–80. In Russian
636 Kushiyama, Y., Honjo, H., Niwa, R., Takanari, H., Yamazaki, M., Takemoto, Y., et al. (2016). Partial i-
637 k1 blockade destabilizes spiral wave rotation center without inducing wave breakup and facilitates
638 termination of reentrant arrhythmias in ventricles. *American Journal of Physiology: Heart and*
639 *Circulatory Physiology* 311, H750–H75
640 Lombaert, H., Peyrat, J., Croisille, P., Rapacchi, S., Fanton, L., Cheriet, F., et al. (2012). Human atlas of
641 the cardiac fiber architecture: Study on a healthy population. *IEEE TRANSACTIONS ON MEDICAL*
642 *IMAGING* 31, 1436–1447
643 MacEdo, P. G., Kapa, S., Mears, J. A., Fratianni, A., and Asirvatham, S. J. (2010). Correlative anatomy for
644 the electrophysiologist: ablation for atrial fibrillation. part ii: regional anatomy of the atria and relevance
645 to damage of adjacent structures during af ablation. *Journal of Cardiovascular Electrophysiology* 21,
646 829–836
647 Mekkaoui, C., Porayette, P., Jackowski, M. P., Kostis, W. J., Dai, G., Sanders, S., et al. (2013). Diffusion
648 mri tractography of the developing human fetal heart. *PLoS ONE* 8, e72795. doi:10.1371/journal.pone.
649 0072795
650 Mines, G. R. (1913). On dynamic equilibrium in the heart. *J. Physiol.* 46, 349–383
651 Nattel, S. (2002). New ideas about atrial fibrillation 50 years on. *Nature* 415, 219–226

Panfilov, A. V., Rudenko, A. N., and Pertsov, A. M. (1984). Twisted scroll waves in active 3-dimensional media. *Doklady AN SSSR* 279, 1000–1002. In Russian

Pellman, J., Lyon, R. C., and Sheikh, F. (2010). Extracellular matrix remodeling in atrial fibrosis: mechanisms and implications in atrial fibrillation. *Journal of Molecular and Cellular Cardiology* 48, 461–467

Pertsov, A. M., Davidenko, J. M., Salomonsz, R., and Baxter, J., W. T. Jalife (1993). Spiral waves of excitation underlie reentrant activity in isolated cardiac muscle. *Circ. Res.* 72, 631–650

Pertsov, A. M., Wellner, M., Vinson, M., and Jalife, J. (2000). Topological constraint on scroll wave pinning. *Phys. Rev. Lett.* 84, 2738–2741

Pervolaraki, E., Anderson, R., Benson, A., Moore, B., Zhang, H., and Holden, A. (2012). Diffusion tensor magnetic resonance imaging of anisotropic and orthotropic architecture of the human foetal ventricular myocardium. *Proc Physiol Soc* 28

Pervolaraki, E., Anderson, R. A., Benson, A. P., Hays-Gill, B., Holden, A. V., Moore, B. J. R., et al. (2013). Antenatal architecture and activity of the human heart. *INTERFACE FOCUS* 3, 20120065

Pervolaraki, E., Dachtler, J., Anderson, R. A., and Holden, A. V. (2017). Ventricular myocardium development and the role of connexins in the human fetal heart. *Scientific Reports* 7, 12272. doi:10.1038/s41598-017-11129-9

Pervolaraki, E., Hodgson, S., Holden, A. V., and Benson, A. P. (2014). Towards computational modelling of the human foetal electrocardiogram: normal sinus rhythm and congenital heart block. *Europace* 16, 758—765

Rodriguez, B., Eason, J. C., and Trayanova, N. (2006). Differences between left and right ventricular anatomy determine the types of reentrant circuits induced by an external electric shock. a rabbit heart simulation study. *PROGRESS IN BIOPHYSICS & MOLECULAR BIOLOGY* 90, 399–413

Smaill, B. H., LeGrice, I. J., Hooks, D. A., Pullan, A. J., Caldwell, B. J., and Hunter, P. J. (2004). Cardiac structure and electrical activation: Models and measurement. *CLINICAL AND EXPERIMENTAL PHARMACOLOGY AND PHYSIOLOGY* 31, 913–919

Spach, M. (2001). Mechanisms of the dynamics of reentry in a fibrillating myocardium - developing a genes-to-rotors paradigm. *CIRCULATION RESEARCH* 88, 753–755

Takemoto, Y., Takanari, H., Honjo, H., Ueda, N., Harada, M., Kato, S., et al. (2012). Inhibition of intercellular coupling stabilizes spiral-wave reentry, whereas enhancement of the coupling destabilizes the reentry in favor of early termination. *American Journal of Physiology: Heart and Circulatory Physiology* 303, H578–H586

Tang, M., Holden, A., Anderson, R., and Pervolaraki, E. (2016). Contrast-enhanced magnetic resonance imaging of the human foetal heart reveals its myocardial architecture. *Proc Physiol Soc* 37

Vigmond, E., Vadakkumpadan, F., Gurev, V., Arevalo, H., Deo, M., Plank, G., et al. (2009). Towards predictive modelling of the electrophysiology of the heart. *EXPERIMENTAL PHYSIOLOGY* 94, 563–577. doi:10.1113/expphysiol.2008.044073

Wellner, M., Berenfeld, O., Jalife, J., and Pertsov, A. M. (2002). Minimal principle for rotor filaments. *PNAS* 99, 8015–8018

Wiener, N. and Rosenblueth, A. (1946). The mathematical formulation of the problem of conduction of impulses in a network of connected excitable elements, specifically in cardiac muscle. *Arch. Inst. Cardiologia de Mexico* 16, 205–265

Winfree, A. T. (1991). Varieties of spiral wave behaviour — an experimentalist's approach to the theory of excitable media. *Chaos* 1, 303–334

696 Workman, A. J., Kane, K. A., and Rankin, A. C. (2008). Cellular bases for human atrial fibrillation. *Heart*
697 *Rhythm* 5, S1–S6
698 Wu, T. J., Yashima, M., Xie, F., Athill, C. A., Kim, Y. H., Fishbein, M. C., et al. (1998). Role of pectinate
699 muscle bundles in the generation and maintenance of intra-atrial reentry. potential implications for the
700 mechanism of conversion between atrial fibrillation and atrial flutter. *Circulation Research* 83, 448–462
701 Yamazaki, M., Mironov, S., Taravant, C., Brec, J., Vaquero, L. M., Bandaru, K., et al. (2012).
702 Heterogeneous atrial wall thickness and stretch promote scroll waves anchoring during atrial fibrillation.
703 *Cardiovascular Research* 94, 48–57
704 Zhu, R., Millrod, M., Zambidis, E., and Tung, L. (2016). Variability of action potentials within and among
705 cardiac cell clusters derived from human embryonic stem cells. *SCIENTIFIC REPORTS* 6, 18544

Figure 2. Anisotropy effect in the 2D slice simulations, time shown under each panel in time units of Eqs. (1)-(2). **a)** *Isotropic conduction*: after the transient first rotation around the septum cuneiform opening, the slow excitation re-entry pins to the sharp low end of the opening in the foetal heart. (Multimedia view) Fig2a.mpg. **b)** *Anisotropic conduction*: after the fast transient first rotation around the septum cuneiform opening, the anisotropy of the foetal heart turns the initial spiral wave into the fast anatomical re-entry around the septum cuneiform opening. (Multimedia view) Fig2b.mpg.

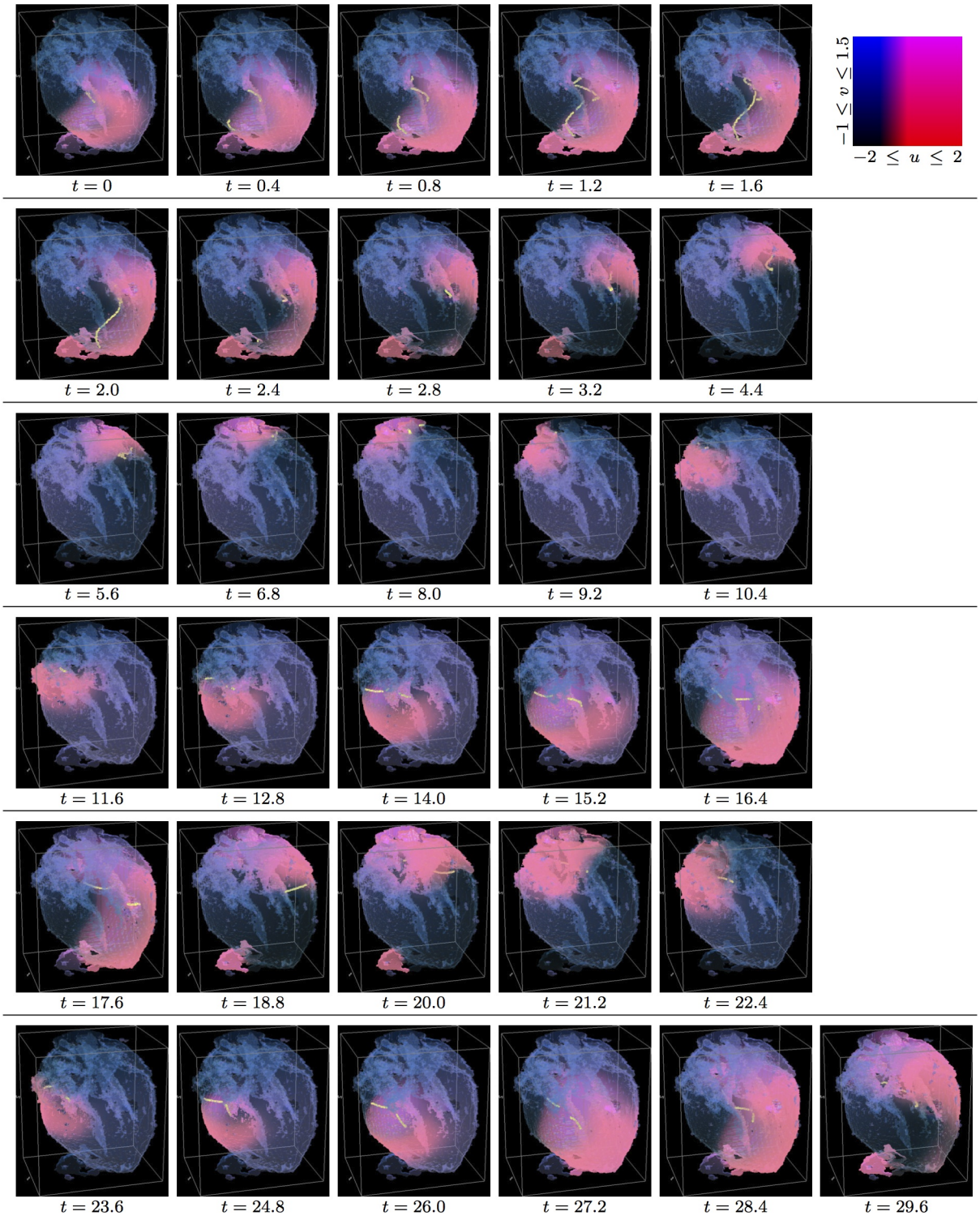

Figure 3. Isotropic whole heart simulation. The translucent foetal heart is shown in blue, excitation front shown in red (see the color box in Figure 3), the yellow lines are the instant organising filaments of the excitation vortices; time shown under each panel in time units of Eqs. (1)-(2). After a short transient the organising filament of the initial vortex breaks into the two short pieces each of which finds its own synchronous perpetual pathway, resulting in the perpetual cardiac re-entry in the foetal heart. (Multimedia view) Fig3.mpg.

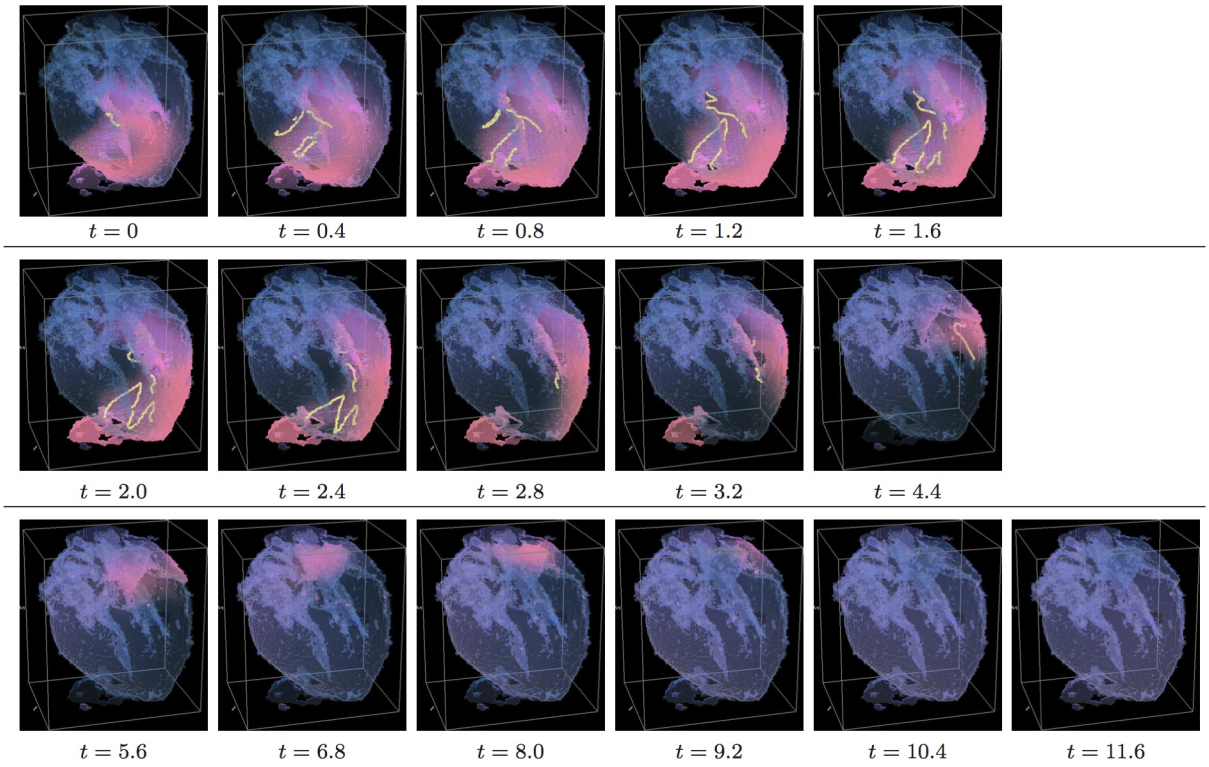

Figure 4. Anisotropic whole heart simulation. The translucent foetal heart is shown in blue, excitation front shown in red (see the color box in Figure 3), the yellow lines are the instant organising filaments of the excitation vortices; time shown under each panel in time units of Eqs. (1)-(2). The anisotropy of the heart causes the fast transient distortion of the organising filament of the initial excitation vortex and drift towards the inexcitable boundary of the heart, ultimately resulting in the very fast self termination of the excitation vortex. (Multimedia view) Fig4.mpg.

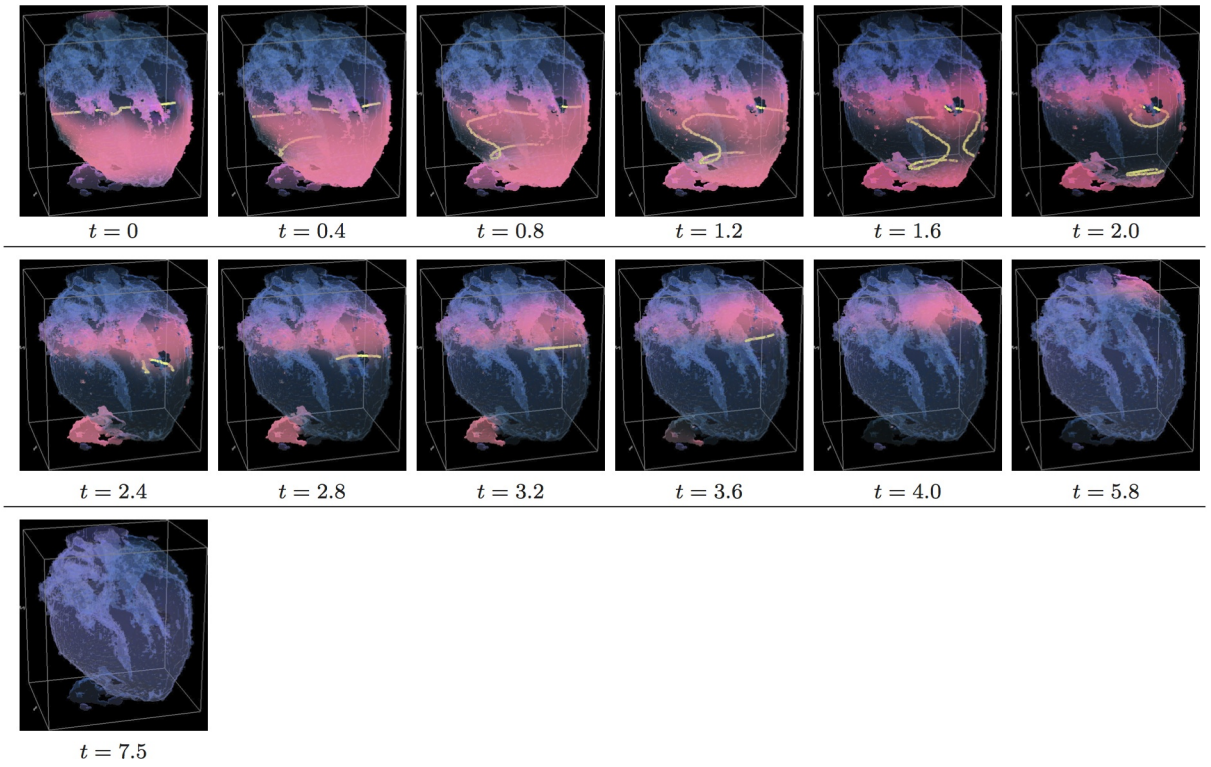

Figure 5. Isotropic whole heart simulation. The translucent foetal heart is shown in blue, excitation front shown in red (see the color box in Figure 3), the yellow lines are the instant organising filaments of the excitation vortices; time shown under each panel in time units of Eqs. (1)-(2). After a short transient the organising filament of the initial vortex breaks into the two pieces each of which fast terminates: one at the base and another at the apex of the heart. (Multimedia view) Fig5.mpg.

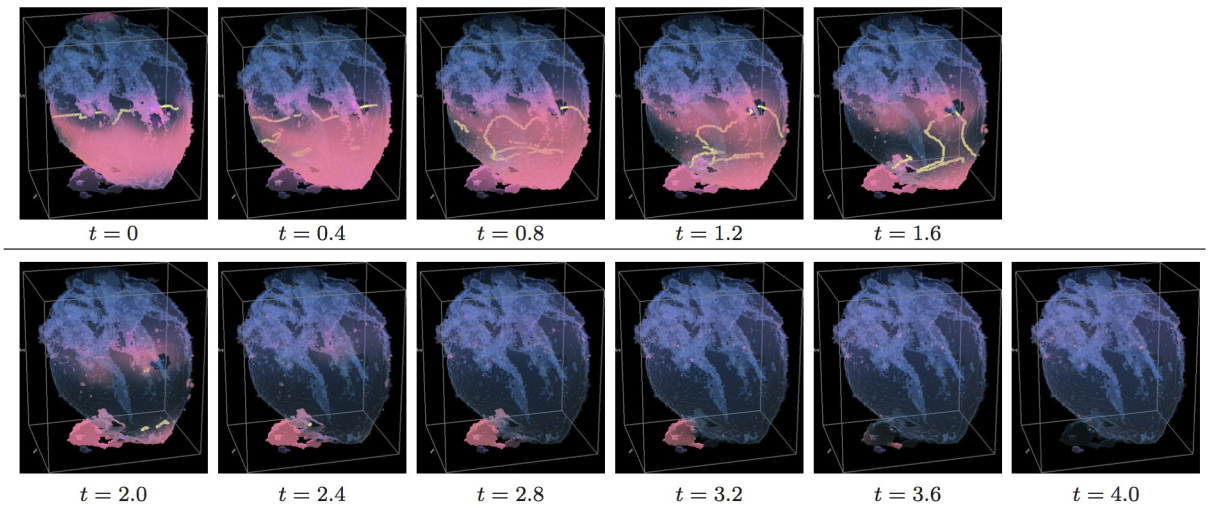

Figure 6. Anisotropic whole heart simulation. The translucent foetal heart is shown in blue, excitation front shown in red (see the color box in Figure 3), the yellow lines are the instant organising filaments of the excitation vortices; time shown under each panel in time units of Eqs. (1)-(2). The anisotropy of the heart causes the fast transient distortion of the organising filament of the initial excitation vortex, followed by the fast drift and self-termination at the apex of the heart. (Multimedia view) Fig6.mpg.

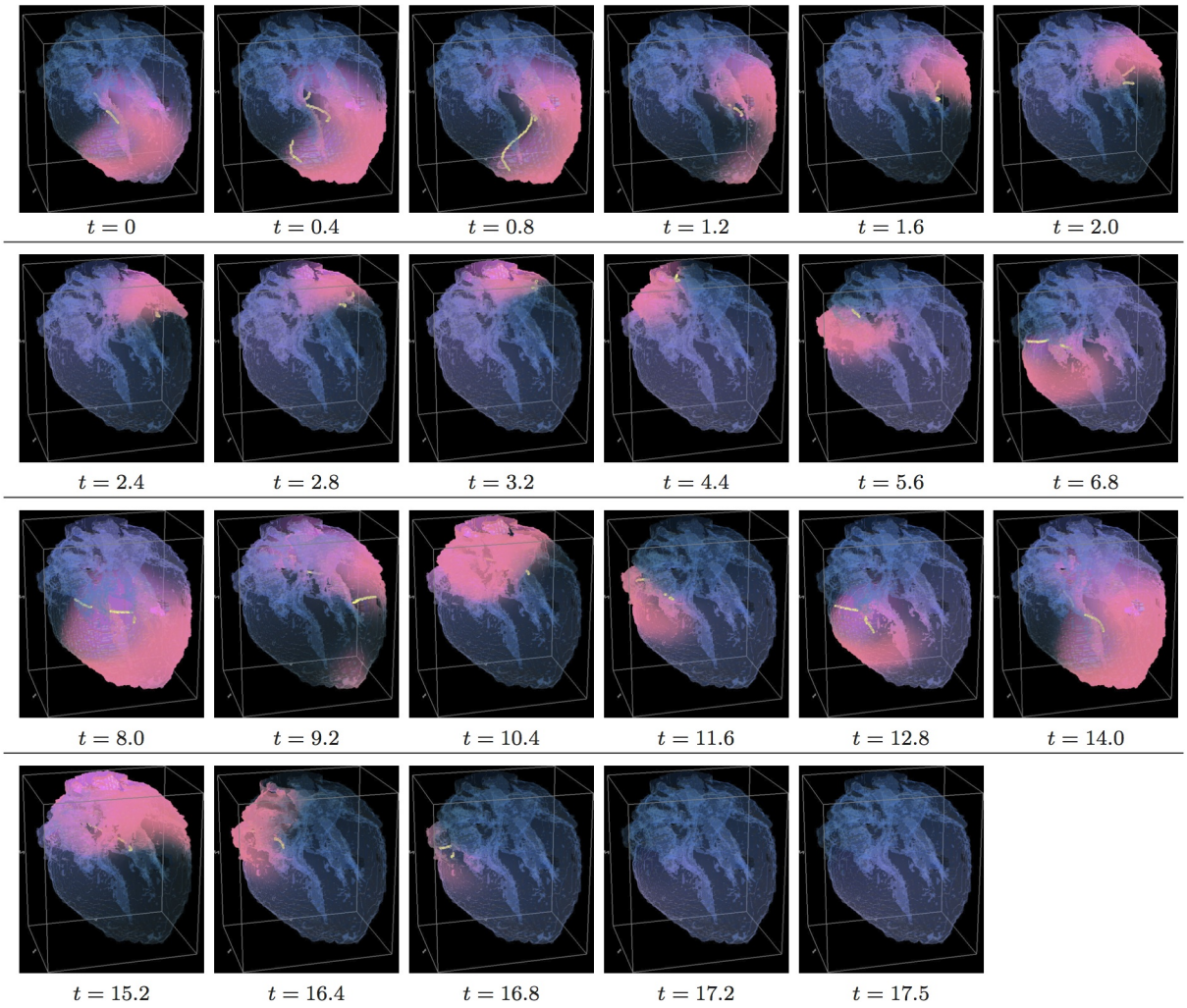

Figure 7. Isotropic "edited" whole heart simulation. The translucent foetal heart is shown in blue, excitation front shown in red (see the color box in Figure 3), the yellow lines are the instant organising filaments of the excitation vortices; time shown under each panel in time units of Eqs. (1)-(2). After a short transient the organising filament of the initial vortex breaks into the two short pieces each of which finds its own synchronous pathway, resulting after a few rotations in the synchronous termination of the filaments in the base of the foetal heart. (Multimedia view) Fig7.mpg.

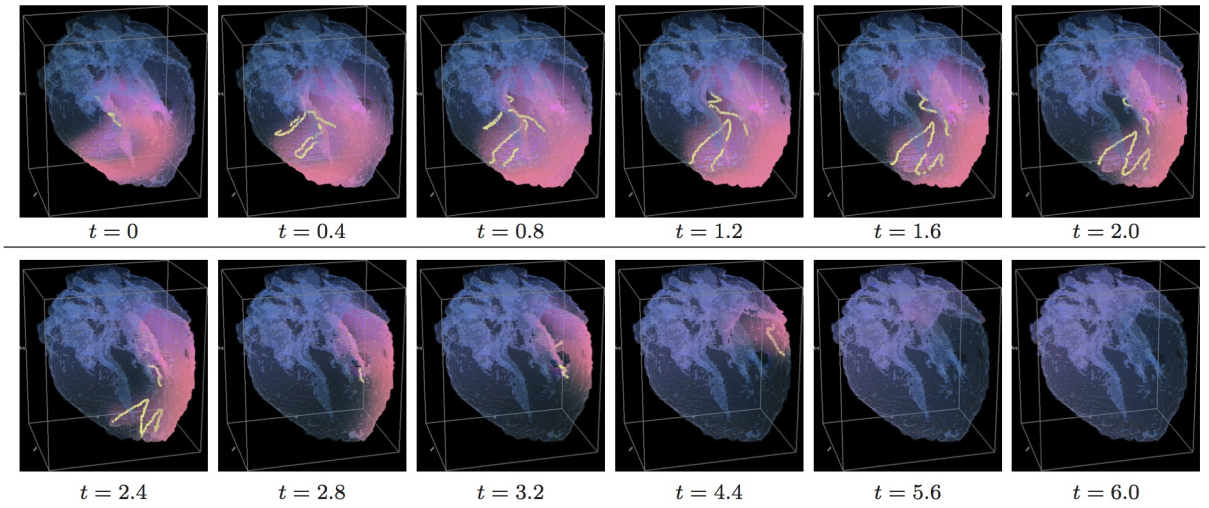

Figure 8. Anisotropic "edited" whole heart simulation. The translucent foetal heart is shown in blue, excitation front shown in red (see the color box in Figure 3), the yellow lines are the instant organising filaments of the excitation vortices; time shown under each panel in time units of Eqs. (1)-(2). The anisotropy of the heart causes the significant transient distortion of the organising filament of the initial vortex, followed by its fast drift towards the apex and the ultimate termination before completing a single rotation. (Multimedia view) Fig8.mpg.

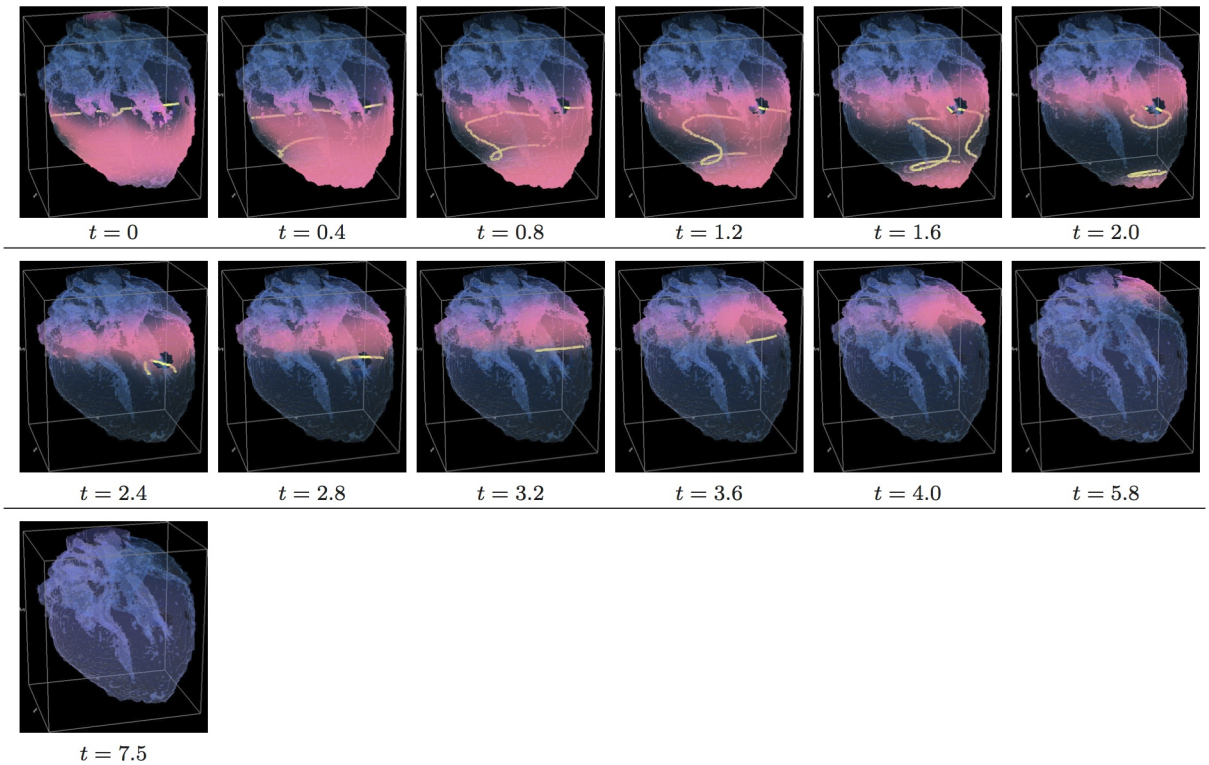

Figure 9. Isotropic "edited" whole heart simulation. The translucent foetal heart is shown in blue, excitation front shown in red (see the color box in Figure 3), the yellow lines are the instant organising filaments of the excitation vortices; time shown under each panel in time units of Eqs. (1)-(2). After a short transient the organising filament of the initial vortex breaks into the two pieces each of which fast terminates: one at the base and another at the apex of the heart. (Multimedia view) Fig9.mpg.

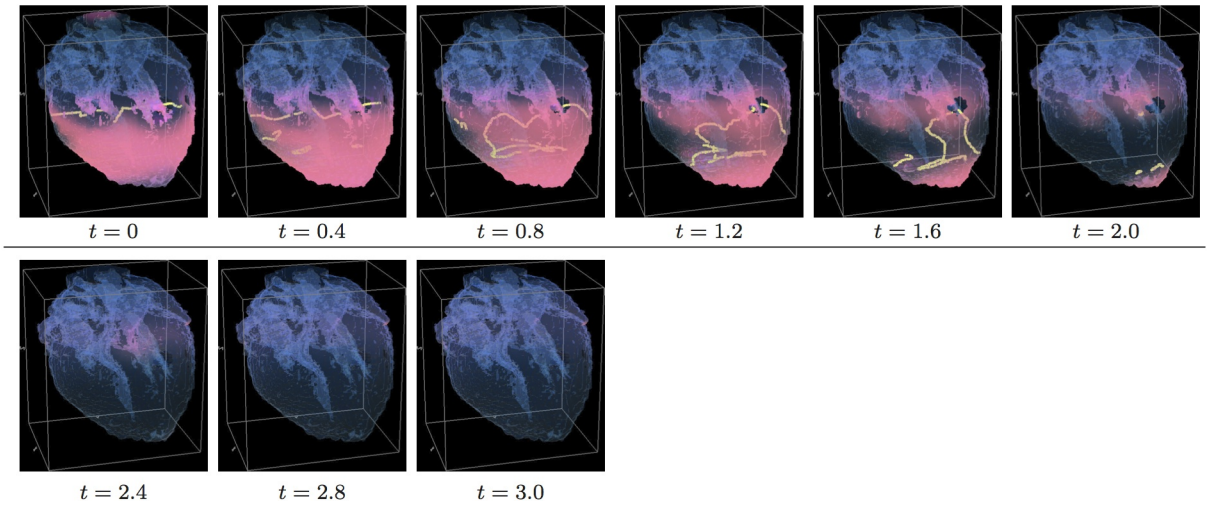

Figure 10. Anisotropic "edited" whole heart simulation. The translucent foetal heart is shown in blue, excitation front shown in red (see the color box in Figure 3), the yellow lines are the instant organising filaments of the excitation vortices; time shown under each panel in time units of Eqs. (1)-(2). The anisotropy of the heart causes the fast significant transient distortion of the organising filament of the initial excitation vortex, followed by the fast drift towards the apex and ultimate termination before the first rotaion has ever started. (Multimedia view) Fig10.mpg.

	Original MRI		"Edited" MRI	
Isotropic	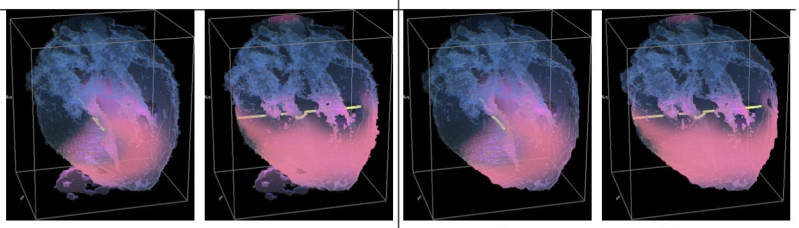			
Simulation FIG.	FIG.3	FIG.5	FIG.7	FIG.9
Filaments Termination time (t.u)	t=∞	t=4.0	t=16.9	t=4.0
Recovery time (t.u)	t=∞	t=7.5	t=17.5	t=7.5
Average $\#\ of\ filaments$	3.4	4.7	3.2	4.7
Average *total length*	29.3	80.5	28.7	82.9
$max(\#\ of\ filaments)(t_{max(\#\ of\ filaments)})$	9 (t=1.0)	12 (t=1.4)	9 (t=0.2)	12 (t=0.5)
$max(total\ length)\ (t_{max(total\ length)})$	127.1 (t=1.6)	188.0 (t=1.5)	122.3 (t=0.7)	190.7 (t=1.5)
AnIsotropic	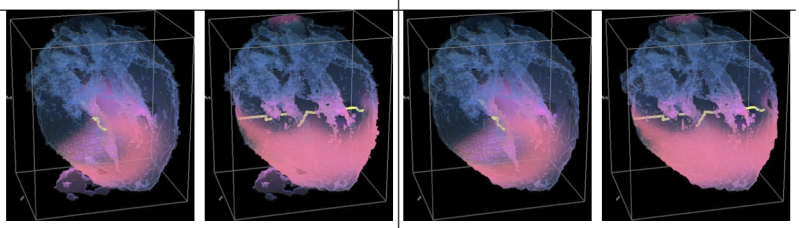			
Simulation FIG.	FIG.4	FIG.6	FIG.8	FIG.10
Filaments Termination time (t.u)	t=5.3	t=2.6	t=4.8	t=2.3
Recovery time (t.u)	t=10.0	t=4.0	t=6.0	t=3.0
Average $\#\ of\ filaments$	6.5	9.5	6.3	10.3
Average *total length*	91.2	152.6	95.4	177.0
$max(\#\ of\ filaments)(t_{max(\#\ of\ filaments)})$	13 (t=0.8)	17 (t=0.5)	17 (t=0.4)	16 (t=0.7)
$max(total\ length)\ (t_{max(total\ length)})$	179.7 (t=1.8)	278.6 (t=0.9)	180.3 (t=0.7)	290.2 (t=1.0)

Figure 11. Whole heart simulation: re-entry termination times. The translucent foetal heart is shown in blue, excitation front shown in red (see the color box in Figure 3), the yellow lines are the instant organising filaments of the excitation vortices. Re-entry self-termination time in time units of Eqs. (1)-(2) is shown under each simulation Figure3–Figure10 initiation panel. Comparison of the respective isotropic (top row) vs anisotropic (bottom row) simulations shows that, regardless of with or without the "leftover" piece, anisotropy results in faster termination of re-entry, and at least twice shorter recovery time. Respective comparison of the original MRI with the corresponding "edited out leftover" simulations shows that the leftover "incidental capacitor" effect, depending of the re-entry location/orientation with respect to the "incidental capacitor" own location/orientation, might significantly prolongate cardiac re-entry life time. The bigger number and the total length of the filaments tend to correlate with the faster termination of re-entry, though these fail to identify persistent re-entry in Figure 3 simulation.

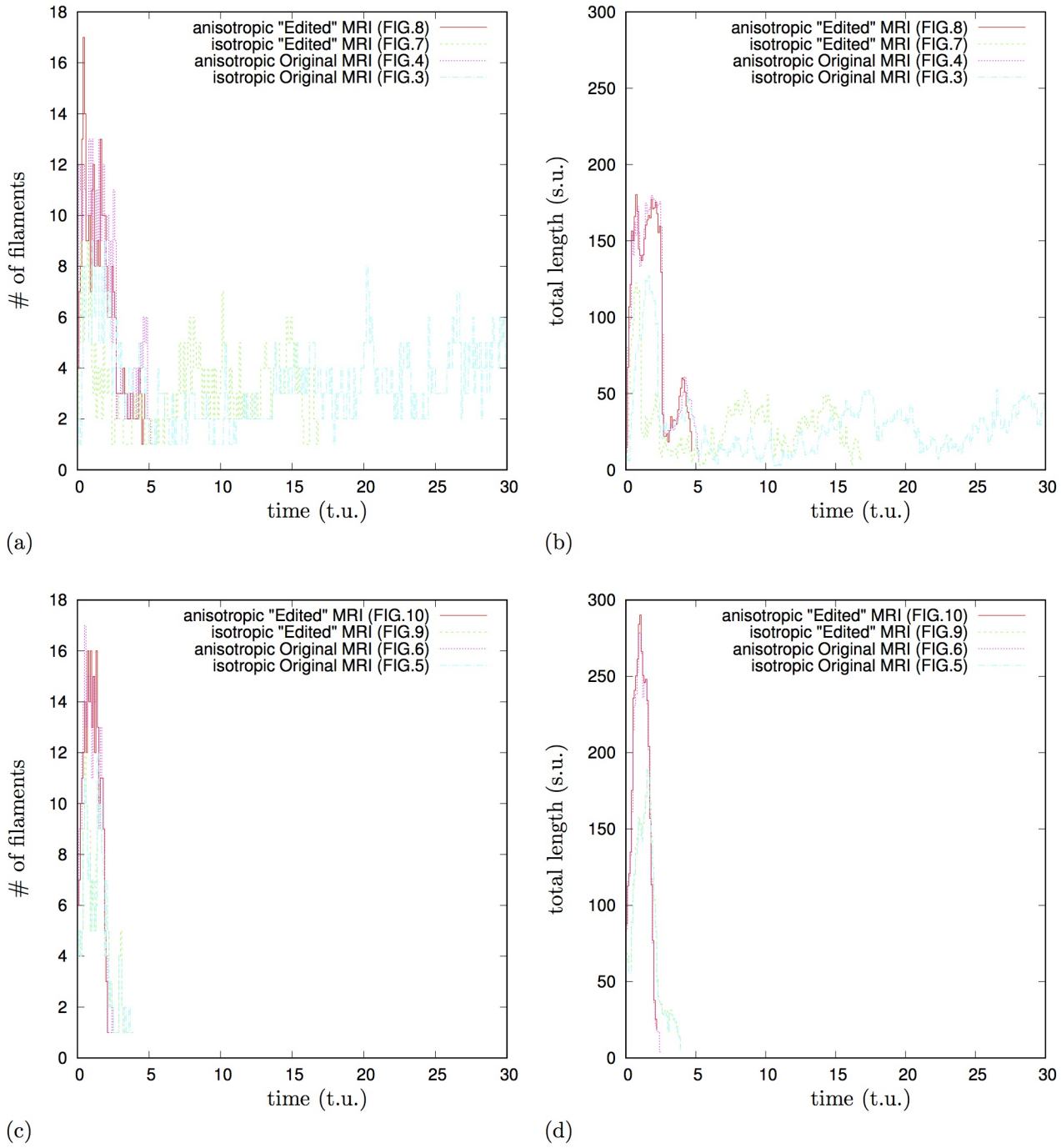

Figure 12. Whole heart simulation: time course of the number of filaments #, and of the total length of the filaments, time and the total length of the filaments shown in the time and space units of Eqs. (1)-(2). **Initial position of the vortex filament *along the* x *axis***, Figure 3, Figure 4, Figure 7, and Figure 8 simulations: **(a)** time course of the number of filaments # ; **(b)** time course of the total length of the filaments. **Initial position of the vortex filament *along the* y *axis***, Figure 5, Figure 6, Figure 9, and Figure 10 simulations: **(c)** time course of the number of filaments # ; **(d)** time course of the total length of the filaments. Anisotropy increases the transient number and the transient total length of the filaments. The bigger transient number and the total length of the filaments tend to correlate with the faster termination of re-entry. The biggest transient total lengths of the filaments was in case of the re-entry initiated *along the* y *axis*, panel **(d)**, which ensured its fastest termination. It can be seen from Figure 5, Figure 6, Figure 9, and Figure 10, that the initial position of the filament *along the* y *axis* allowed it to grow intramurally, thus maximally increasing the transient total length of the filaments, and speeding up their termination.